On-Chip Feedthrough Cancellation Methods for Microfabricated AFM Cantilevers With Integrated Piezoelectric Transducers

M. Bulut Coskun, Anthony G. Fowler, *Member, IEEE*, Mohammad Maroufi, *Member, IEEE*, and S. O. Reza Moheimani, *Fellow, IEEE*

***Abstract*— Active microcantilevers with on-chip sensing and actuation capabilities provide significant advantages in tapping-mode atomic force microscopy. The collocated transduction in active cantilevers enables effective control of their dynamics, allowing for the modification of the quality (Q) factor and operation at higher flexural modes to obtain higher scan rates. However, having closely spaced transducers in dynamic applications often results in electrical crosstalk from the actuation signal to the sensor output. As a result, the dynamic response of the cantilever becomes heavily dominated by this feedthrough, making the use of on-chip transduction impractical for atomic force microscope (AFM) imaging without cancelling this undesired effect. In this paper, we propose two on-chip feedthrough cancellation methods based on pseudo-differential actuation and differential sensing concepts. The implementation of the methods is demonstrated by the use of two microfabricated cantilevers with separate piezoelectric sensors and actuators. Following the cancellation of the feedthrough, both cantilevers are successfully employed for AFM imaging using the on-chip transducers for actuation and deflection sensing. [2017-0101]**

***Index Terms*— Atomic force microscopy, piezoelectric microcantilevers, feedthrough cancellation, psuedo-differential actuation, differential sensing, imaging.**

I. Introduction

OVER RECENT decades, the atomic force microscope (AFM) has been proven to be a versatile and powerful scientific instrument that has performed a central role in numerous nanoscale applications [1]–[5]. Among the AFM's different modes of operation, tapping-mode AFM has found widespread use, and is especially preferred over contact mode while working with delicate samples [6], [7]. In typical tapping-mode AFM operation, a cantilever with a sharp tip is excited by a base shaker at its fundamental mode with a set oscillation amplitude, while intermittently contacting a surface. In this state, the cantilever is scanned over the sample's surface by the use of an in-plane XY positioner. The conventional way to measure the oscillation amplitude is through the use of the optical lever method, which involves using a photodetector to measure the position of a laser reflected off the cantilever surface. Encountering a topology variation during the AFM scan creates a transient change in the tip-sample interaction forces, which correspondingly alters the oscillation amplitude of the cantilever. The resulting change in the demodulated deflection signal is fed back to the Z-axis controller, which drives the out-of-plane positioner to maintain the oscillation amplitude of the cantilever at its setpoint. Hence, the three-dimensional surface topography of the sample can be estimated using the controller output combined with the lateral position of the XY positioner.

Improving this well-established operation's versatility and performance to meet the demands of newly emerging application areas has been a significant driver of research in the field. There is especially a growing interest in the development of active cantilevers that contain integrated collocated actuators and/or sensors [8]–[20], which offer several advantages over the conventional approach.

On-chip sensing allows bypassing of the bulky laser measurement system, which simplifies the operation of the AFM due to the need for frequent alignment of the laser position [9], [17]. With integrated sensors, it is also possible to implement cantilever arrays [14], [15] to increase the throughput of the AFM by enabling parallel scanning, which would otherwise require a separate laser/photodetector for each cantilever [21]. Additionally, the layout of the sensors on the cantilever can be optimally designed to maximize the displacement sensitivity at certain modes of interest [22].

Integrated actuation mechanisms similarly provide many potential advantages. Whereas cantilever excitation using a base shaker introduces significant distortion and noise in the frequency response [23], on-chip actuation provides a significantly cleaner frequency response over a wide range, which enables the use of system identification techniques. Importantly, the combination of on-chip sensing and actuation enables effective control of the cantilever dynamics. This includes manipulating the cantilever's quality (Q) factor [24]–[26] and facilitating imaging at higher modes of oscillation for faster scanning [18].

The concept of active cantilevers is also a vital step to developing an on-chip implementation of the AFM [27], [28]. In this case, the goal is to introduce a system that retains the functionality of its macroscale counterpart, but with a

Manuscript received May 1, 2017; revised July 2, 2017; accepted July 19, 2017. Subject Editor C. Rembe. *(Corresponding author: M. Bulut Coskun.)*

The authors are with the Department of Mechanical Engineering, University of Texas at Dallas, Richardson, TX 75080 USA (e-mail: bulut.coskun@utdallas.edu; anthony.fowler@utdallas.edu; mohammad.maroufi@utdallas.edu; reza.moheimani@utdallas.edu).

Color versions of one or more of the figures in this paper are available online at http://ieeexplore.ieee.org.

Digital Object Identifier 10.1109/JMEMS.2017.2731762

significantly lower size and cost due to the benefits of microelectromechanical systems (MEMS)-based fabrication. In [28], we demonstrated a silicon-on-insulator (SOI) on-chip AFM, which comprises a high-precision in-plane nanopositioner for positioning of an integrated AFM cantilever. This system has the potential to provide on-chip video-rate AFM owing to the high operating bandwidth of MEMS nanopositioner, and the ability to control the cantilever dynamics.

Despite these merits, microcantilevers and similar micro/nano resonator systems with closely spaced integrated transducers commonly suffer from crosstalk from the actuation signal to the sensor output. This is primarily due to the presence of parasitic capacitances through the devices' dielectric layers and substrate, and is commonly referred to as feedthrough. As the sensing elements become smaller, the combination of the parasitic capacitances originating from the actuation and sensing electrodes, routing tracks, bonding pads, wiring, and readout circuity become comparable to the capacitances of the sensing elements [29]. Feedthrough has the effect of concealing the inherent dynamics of the cantilever and drastically reducing the signal-to-noise ratio. This effect becomes even more pronounced at higher frequencies as capacitive feedthrough exhibits high-pass characteristics.

To date, a number of feedthrough cancellation methods have been practiced for microscale devices including resonators [30], [31] and nanopositioners [32]. In [30], a MEMS resonator implementing a dummy electrode was driven by a phase-inverted version of the actuation signal. As the parasitic impedances associated with the actual actuator and the dummy actuator were closely matched, this mechanism resulted in effective cancellation of the feedthrough seen in the sensor signal. Furthermore, modification of the on-chip routing of the actuation and sensing signals to mitigate the feedthrough and improve the sensing bandwidth is also practiced in an in-plane MEMS nanopositioner in [32].

Regarding feedthrough in active AFM cantilevers, [12] proposes a cancellation method for a cantilever with thermal actuation and piezoresistive sensing. According to this principle, when a sinusoidal voltage input with a frequency of ω is applied to a thermal actuator, the cantilever is simultaneously excited at frequencies of ω and 2ω. Utilizing this inherent property, feedthrough from the thermal actuators to piezoresistive sensors is reduced by exciting the system and sensing the displacement at different frequencies. However, the application of this method is limited to thermal actuators. Another active AFM probe is demonstrated in [33], where an external reference capacitor is used in conjunction with a variable gain to implement a capacitance compensation mechanism. Here, the ability to effectively estimate the dynamics of the feedthrough using a fixed capacitor is potentially limited, especially while canceling higher modes.

A number of approaches have also been demonstrated that aim to model the frequency-dependent dynamics of the electrical feedthrough to provide more accurate cancellation. In [16], a field programmable analog array (FPAA) was used to implement a transfer function representing the feedthrough, while a feedforward compensation approach using discrete analog components was shown in [18]. This, however is potentially laborious and requires prior knowledge of the feedthrough dynamics.

Among all the methods, on-chip feedthrough cancellation concepts potentially provide an effective and straightforward means of accurately compensating for the feedthrough present in a given microfabricated device.

In this work, we demonstrate two on-chip feedthrough cancellation methods on two microfabricated cantilevers that feature integrated piezoelectric sensors and actuators. The proposed techniques are based on pseudo-differential actuation and differential sensing concepts, which do not require complex readout circuits while offering fast, simple, and effective cancellation of the feedthrough. Subsequent to the cancellation, both cantilevers are successfully employed for AFM imaging using the on-chip transducers.

II. Cantilever Design and Microfabrication

A. Cantilever Geometry and Actuator/Sensor Design for On-Chip Feedthrough Cancellation

In order to implement the on-chip feedthrough cancellation techniques, a cantilever design with double-section geometry is chosen. The cantilever is composed of a relatively large planar body ($390\,\mu\text{m} \times 280\,\mu\text{m} \times 5\,\mu\text{m}$) that provides sufficient space to implement multiple piezoelectric transducer configurations, along with physically separate signal routing for each transducer. A smaller rectangular section ($130\,\mu\text{m} \times 75\,\mu\text{m} \times 5\,\mu\text{m}$) containing a probe tip for AFM imaging extends from the larger section. The proposed pseudo-differential actuation and differential sensing methods have been implemented on cantilevers with similar mechanical design and distinct piezoelectric/electrode configurations. In this paper, Type I refers to the pseudo-differentially actuated cantilever, while Type II refers to the cantilever with differential sensing.

The Type I cantilever features three geometrically identical active elements, namely a piezoelectric actuator, a piezoelectric sensor, and a metal electrode (pseudo actuator). As depicted in Fig. 1a, the actuator and the pseudo actuator are placed symmetrically with respect to the piezoelectric sensor, with the aim of creating identical parasitic capacitances between the sensing electrode and each of the actuation electrodes. With this configuration, driving the pseudo actuator with a 180° out-of-phase version of the actuation signal has the effect of negating the primary feedthrough from the main actuator to the sensor. While this approach ideally cancels the feedthrough within the boundaries of the cantilever, additional parasitic impedances originating from the chip body, wiring, and circuitry are compensated by adding an external gain to adjust the signal driving the pseudo actuator to maximize the feedthrough cancellation. A block diagram representation of this mechanism is shown in Fig. 1b.

The Type II cantilever consists of three parallel piezoelectric transducers extending from the base of the cantilever toward its tip, as shown in Fig. 1c. The bottom and top electrodes of each piezoelectric transducer are physically separated. Here, the middle transducer is used for actuation, whereas the

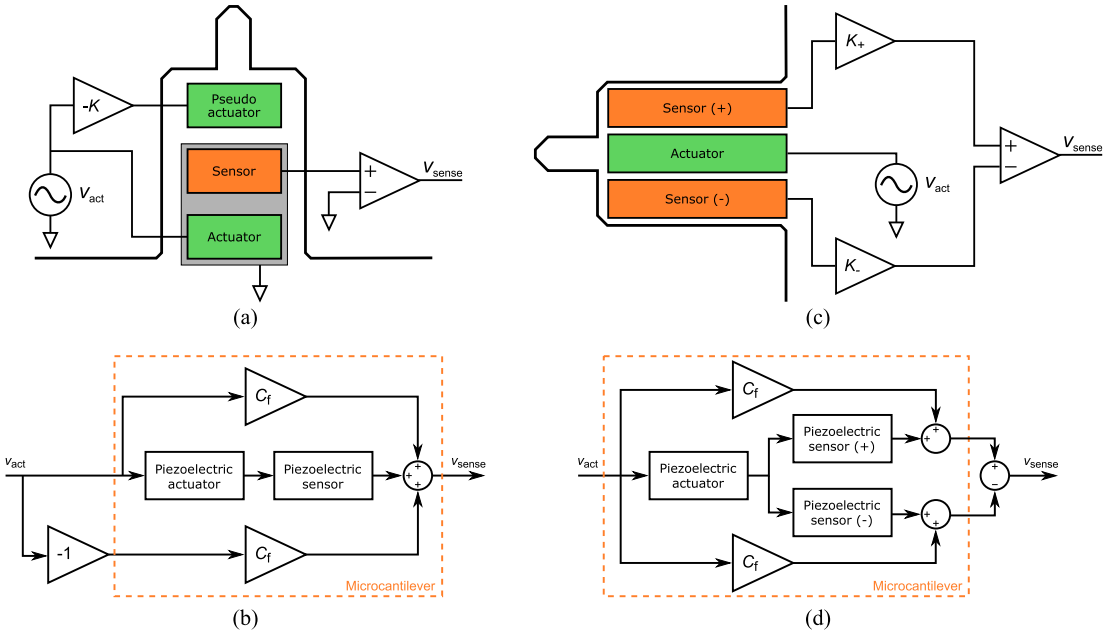

Fig. 1. Schematic diagrams of the actuation and sensing configurations for the microcantilevers, and block diagram representations of their respective feedthrough cancellation mechanisms. (a) and (b) refer to the Type I cantilever, while (c) and (d) refer to the Type II cantilever.

transducers on the left and right sides are employed in a differential sensing configuration by reversing the polarity of the electrical connections to one of the sensors. In this configuration, the induced strain within the cantilever results in the sensors providing induced voltage outputs that have opposite polarities. As the electrical feedthrough from the actuator to each sensor manifests as a common-mode signal, employing a differential amplifier at the output significantly reduces the final level of feedthrough present in the sensor signal. Adjustable gains are implemented at the output of each piezoelectric transducer to allow for fine tuning of the relative sensor amplitudes prior to differential amplification.

B. Microfabrication of the Cantilevers

Both the Type I and Type II cantilevers share the same microfabrication process flow. A silicon-on-insulator (SOI) substrate has been used for the fabrication which is, from top to bottom, composed of a 5-μm-thick Si device layer that defines the cantilever thickness, a 2 μm-thick buried oxide (BOX), and a 450 μm-thick Si handle layer.

The microfabrication of the cantilevers starts with the wet thermal oxidation of the Si device and handle layers at 1000 °C for 35 min. This results in the growth of a 300 nm-thick low-stress oxide layer which primarily serves as an insulation layer on top of the device layer for the current-carrying elements to be deposited in the forthcoming steps. Next, the patterns of the bottom routing elements including the bonding pads, routing tracks, and bottom electrode of the piezoelectric material are transferred via photolithography. Then, the metal layer for the bottom electrode (a 15 nm/150 nm-thick Ti/Pt stack) is evaporated and lifted-off (Fig. 2a). For the piezoelectric elements employed as separate sensors and actuators, a 1 μm-thick AlN layer is first sputtered, followed by the deposition of a 300 nm-thick SiO_2 layer through plasma-enhanced chemical vapor deposition (PECVD), which will

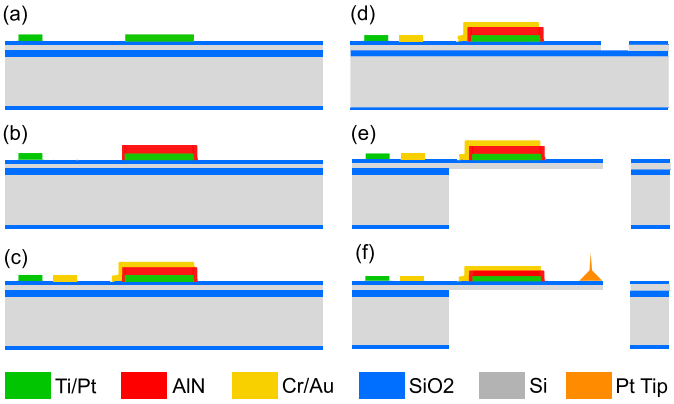

Fig. 2. Microfabrication process flow of the cantilevers: (a) E-beam evaporation of the bottom electrodes (Ti/Pt) and lift-off, (b) AlN sputtering and etching, (c) e-beam evaporation of the top electrodes (Cr/Au) and lift-off, (d) RIE and DRIE etching of the thermal oxide and Si device layers, respectively, (e) backside etching and release, (f) FIB tip deposition.

be used as an etch mask to pattern the AlN. To define the stacked AlN layers on top of the bottom Ti/Pt electrodes on the cantilever, the SiO_2 layer is patterned through lithography and dry etched by Reactive Ion Etching (RIE). This is followed by the selective etching of the AlN layer by Cl_2-based RIE etching and later a short wet etching step inside 2.5 % tetramethylammonium hydroxide (TMAH) solution at 80 °C to guarantee the complete removal of the AlN from the unmasked areas (Fig. 2b). After the removal of the PECVD oxide etch mask by RIE etching, the top routing elements including the bonding pads, routing tracks, sensor/actuator top electrodes, and the pseudo actuator have been transferred, evaporatively deposited (Cr/Au, 20 nm/500 nm), and lastly lifted-off (Fig. 2c). As the final process for the device layer of the SOI wafer, the cantilever geometry is defined by photolithography and etched via Deep Reactive Ion Etching (DRIE) (Fig. 2d). To protect the frontside features

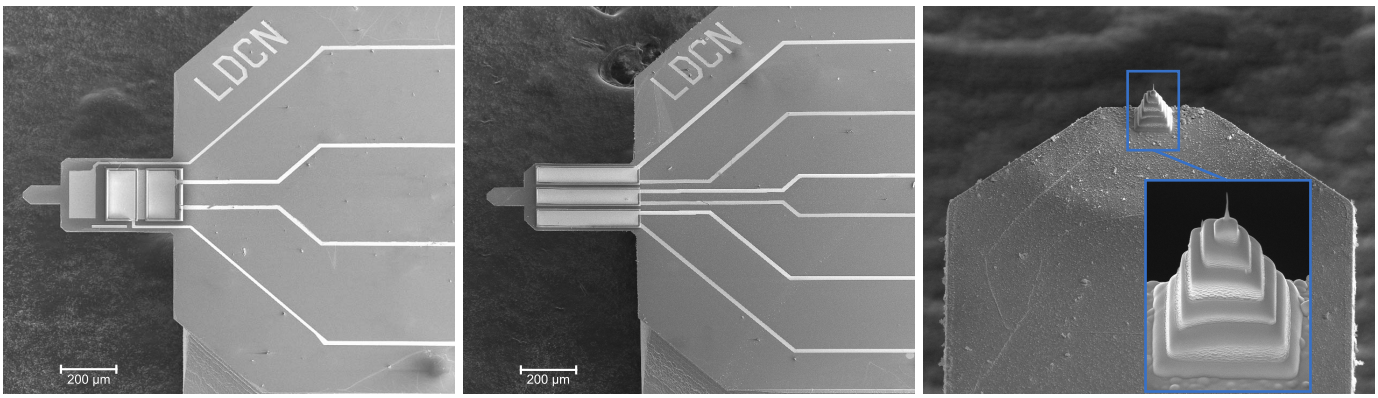

(a) (b) (c)

Fig. 3. SEM images of the microfabricated cantilevers. (a) Type I cantilever. (b) Type II cantilever. (c) FIB-deposited probe tip for AFM imaging.

during the backside etching, the device layer is covered by a 500 nm-thick parylene film. Having protected the frontside, the wafer is flipped and the backside etch-mask features are transferred to a thick photoresist film. The backside etching processes include the etching of the thermal oxide layer, handle layer Si, and BOX layer to release the cantilevers, by the use of RIE, DRIE, and RIE, respectively (Fig. 2e). This is followed by the removal of the parylene film, O_2 plasma cleaning, and dicing of the devices.

For AFM imaging, a Pt probe tip with 10 μm height and a radius of around 30 nm is deposited with the use of an FEI Nova Nanolab 200 focused ion beam (FIB) system (Fig. 2f). A stepped supporting structure is initially deposited using ion beam deposition, while the final tip used for imaging is fabricated through electron beam induced deposition. The fabricated devices are wire bonded to a pin-grid-array (PGA) package for experimental characterization. Scanning electron microscope (SEM) images of the devices and the tip are presented in Fig. 3.

III. Experimental Characterization

A. Mechanical Characterization

The stiffness of AFM cantilevers at their resonance modes has a crucial effect on their imaging performance. In order to experimentally determine the stiffness of AFM cantilevers, two approaches are mainly used in the literature: the Sader method and the thermal noise method [34]. Here, since the fabricated microcantilevers are not perfectly rectangular and also feature a tip, the thermal noise method can provide a better estimation while its implementation is also more straightforward [34], [35].

To implement the thermal noise method, the power spectral density (PSD) of the velocity of the cantilevers at their tip due to the thermal noise is measured using a Polytec MSA-100-3D Micro System Analyzer (MSA). The PSD is then obtained using the MSA's built-in software, and is normalized with respect to its peak value (P_m) observed within the frequency range from 46 kHz to 54 kHz. To obtain the frequency, Q-factor, and stiffness of the cantilevers at their first mode, a Lorentzian function is fitted to the experimental PSD data.

TABLE I
Cantilever Parameters for the First Mode

Cantilever Design	Res. Freq. (kHz)	Q-factor	Stiffness (N/m)
Type I	49.1	334.0	7.4
Type II	49.7	397.2	8.8

The resonance frequencies, Q-factors, and stiffnesses of these cantilevers are reported in Table I. The calculated stiffnesses are consistent with the static stiffness of these cantilevers, which are approximately 10 N/m as obtained using a finite element model in CoventorWare.

B. Frequency Responses and Mode Shapes

The frequency responses of the Type I and II cantilevers from the actuation voltage to the tip displacement are obtained using the MSA. During these experiments, a broadband periodic chirp signal is applied to the integrated piezoelectric actuators while the out-of-plane vibration of the tip is measured (Fig. 4). As expected, both types exhibit comparable frequency responses due to having similar mechanical designs.

The results show that the fundamental modes of the Type I and II cantilevers are located at 49.1 kHz and 49.7 kHz, respectively. For both types, the second to fourth modes lie within the range of 196 kHz - 685 kHz with slight differences. It is noteworthy that as the vibration data is acquired from a single point near the tip, only the bending modes are observable in the obtained frequency responses, while the torsional modes of the cantilever within the experimental bandwidth are not apparent. In order to obtain the mode shapes at these four resonances, the MSA is employed to obtain a series of frequency responses across the cantilever surface. The mode shapes acquired from these experiments, together with their associated resonance frequencies, are presented in Fig. 5. All of these modes can potentially be used for imaging, provided that the lower modes are damped.

As the laser signal is not susceptible to electrical feedthrough, the mechanical responses of the cantilevers are clearly captured by the use of the MSA. In contrast, when the experiments are repeated with the use of the on-chip piezoelectric sensors to measure the tip motion, the dynamics

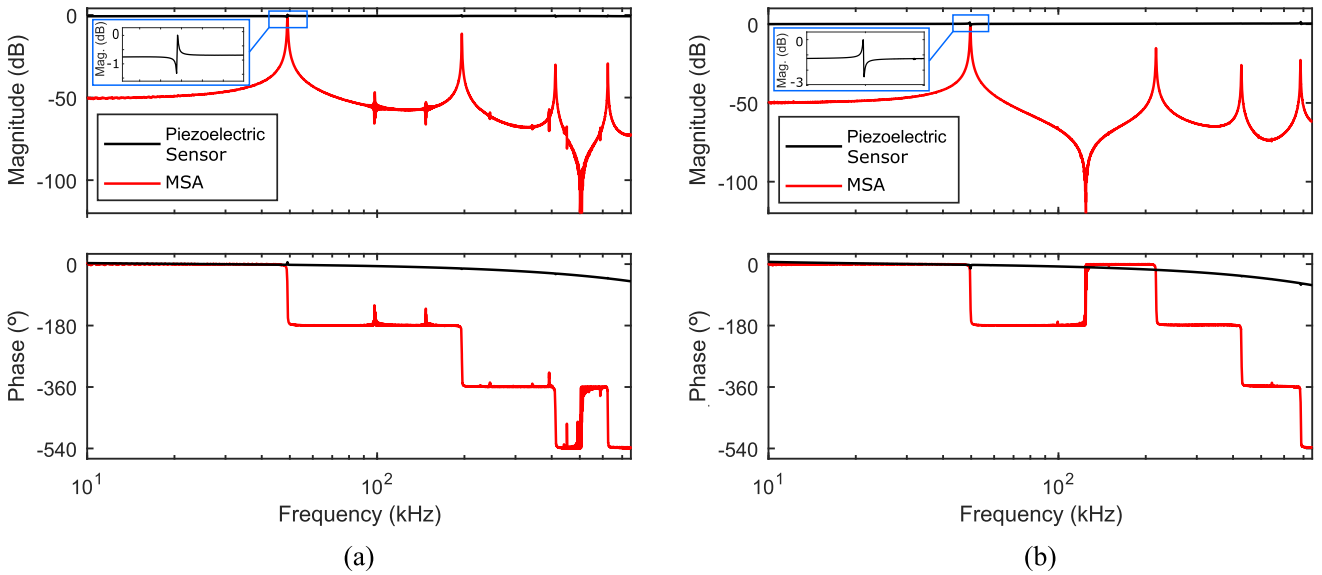

Fig. 4. Comparison between the frequency responses of both (a) Type I and (b) Type II cantilevers, obtained from the actuation voltage to the tip displacement using the MSA and the on-chip piezoelectric sensors. The magnitudes of the first resonance peaks are normalized to 0 dB for comparison purposes. Insets show close-up views around the fundamental mode of the cantilevers.

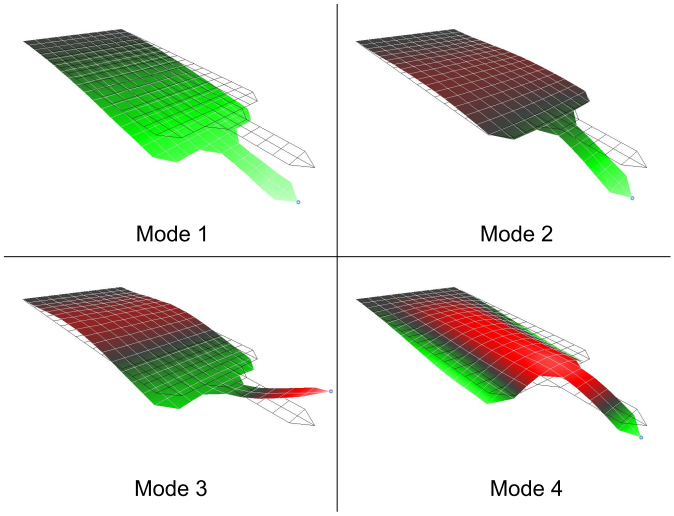

Fig. 5. First four flexural mode shapes of the fabricated microcantilevers, obtained experimentally using the MSA.

of both cantilevers are concealed by the feedthrough. This is also demonstrated by the frequency responses shown in Fig. 4a and 4b, where a Zurich Instruments HF2LI lock-in amplifier is used to drive the cantilevers using a swept-sine excitation while the deflection is measured by the integrated sensors. In this case, the dynamic range of the Type I and II cantilevers obtained at the first mode becomes extremely small compared to the MSA results, being 0.67 dB and 1.01 dB, respectively. The higher modes suffer from similarly low dynamic range. This makes the use of on-chip sensors for AFM imaging highly impractical without compensation for the feedthrough.

IV. Implementation of the On-Chip Feedthrough Cancellation Methods

The proposed on-chip cancellation techniques described in Section II-A have been implemented primarily to nullify the feedthrough at the first mode of the cantilevers. To assess the effectiveness of the feedthrough cancellation techniques over a wider frequency range, the dynamic range of the sensing signal at the higher modes of the cantilever are also measured while the gains of the circuits are tuned for maximum feedthrough cancellation at the first mode.

A. Pseudo-Differential Actuation

To implement the pseudo-differential actuation technique for the Type I cantilevers, a polarity-inverted version of the actuation signal is applied to the pseudo actuator with an adjustable gain. The frequency response of the cantilever is then monitored while increasing the gain of the signal applied to the pseudo actuator. As shown in Fig. 6, as the gain is increased, the feedthrough starts to become partially compensated. When the relative gain applied to the pseudo-actuation signal is tuned to 1.28, the effect of the parasitic impedances are minimized (as shown in red) and the dynamic range and phase at the resonance reach 20.3 dB and $-90°$, respectively. Further increases in the gain beyond this point lead to overcompensation, and the sensor output starts to again be increasingly affected by the feedthrough originating from the pseudo-actuator signal.

Furthermore, the dynamic range of the higher modes are observed when the feedthrough is maximally compensated at the first mode. Fig. 6c shows that under this condition, the dynamic range at the higher modes is less than 3.8 dB. This suggests that the pseudo-differential actuation method should be tuned to cancel feedthrough at the mode of interest.

B. Differential Sensing

For the differential sensing concept, the outputs of the cantilever's two piezoelectric sensors at the fundamental mode are initially observed separately. In this configuration, both the top and bottom electrodes of the piezoelectric

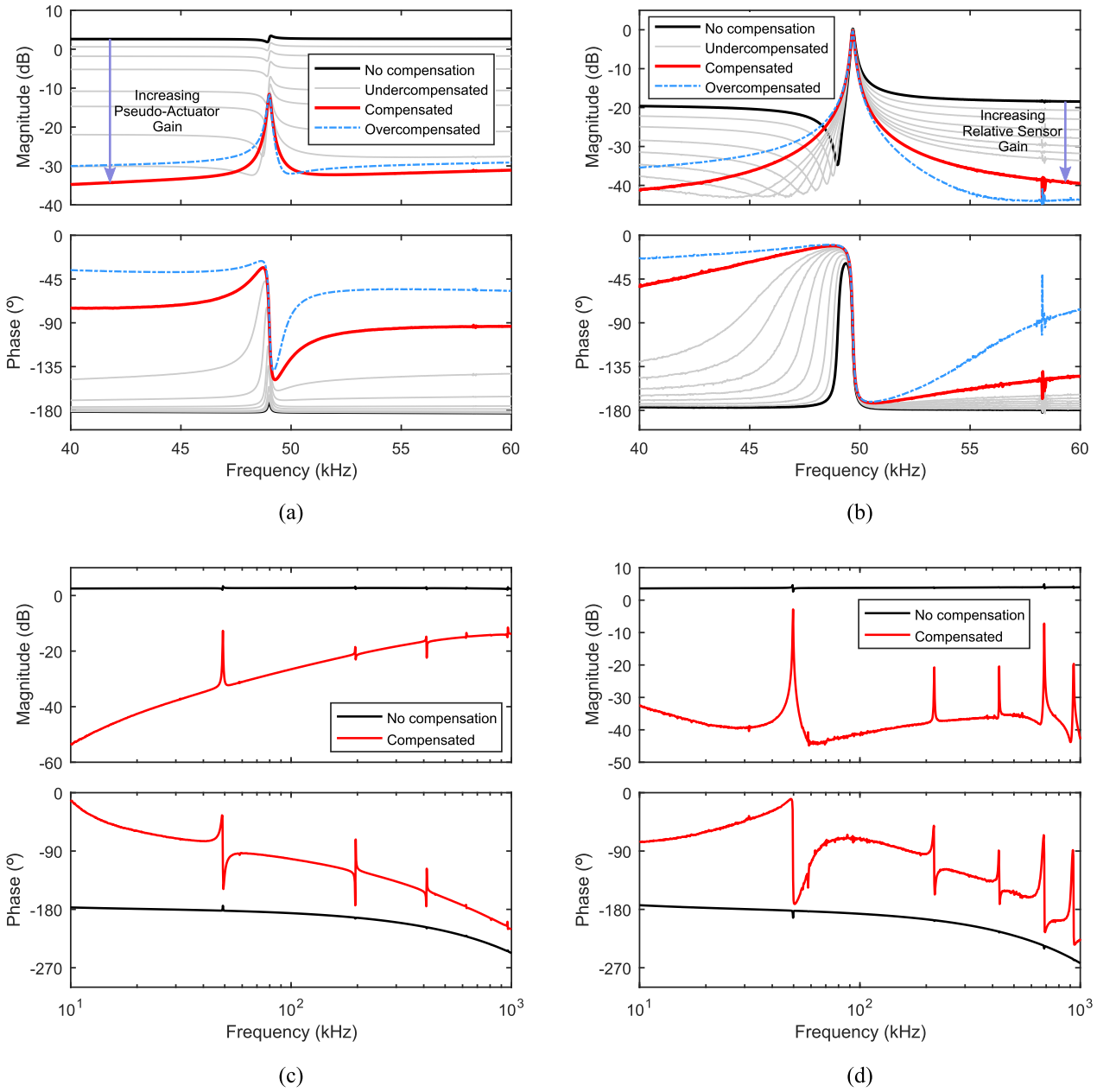

Fig. 6. Cancellation of the feedthrough at the fundamental mode of the (a) Type I and (b) Type II cantilever using the pseudo-differential acutation and differential sensing methods. Frequency response from 10 kHz to 1 MHz for the (c) Type I and (d) Type II cantilever before and after feedthrough cancellation is tuned for the first resonance mode.

sensors are separately accessible via bonding pads. These electrodes are electrically configured such that the outputs of the sensors have opposite polarities, as shown in Fig. 7. Both sensing piezos exhibit similar magnitude and phase, confirming that the piezoelectric characteristics of the sensors are comparable. As expected, the cantilever dynamics are dominated by feedthrough, which results in an extremely small dynamic range at the first mode of 1.2 dB and 1.7 dB for the left and right sensors, respectively.

In order to realize the differential sensing-based feedthrough cancellation concept, the sensor outputs are connected to non-inverting amplifiers with adjustable gains, with the outputs of the amplifiers then being connected to the inputs of a differential amplifier with a gain of 100 V/V. The integrated sensors are used to obtain frequency responses of the cantilever by driving the actuation piezo with a sine-sweep signal generated by the HF2LI lock-in amplifier. The relative gains of the amplifiers at the piezoelectric sensor outputs are initially set to 1. Fig. 6b shows that even in the absence of any tuning, the differential signal already has significantly reduced feedthrough, with the dynamic range of the differential signal reaching 17.3 dB in a partially compensated state. The desired effect of maximizing the level of feedthrough reduction is achieved by increasing the relative gain of the positive sensor output to 1.38. At this point, the dynamic range and the phase at the first resonance is measured to be 34.7 dB and $-90°$, respectively.

Next, the dynamic range of the higher modes are investigated when the feedthrough is compensated for the first mode. As shown in Fig. 6d, the common-mode signal rejection

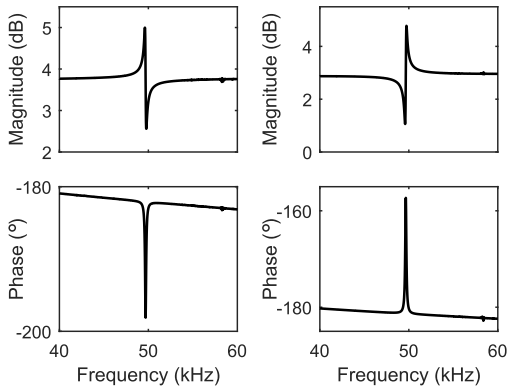

(a) (b)

Fig. 7. Frequency response of the (a) left and (b) right sensors of the Type II cantilever around the first mode.

provided by the differential sensing approach enables a significant reduction in the feedthrough present in the sensor signal, even at higher frequencies. The dynamic ranges from the second to the fourth modes are measured to be 16.6 dB, 15.9 dB, and 30.9 dB, respectively.

C. Comparison of the Feedthrough Cancellation Methods

It has been demonstrated that both the pseudo-differential actuation and differential sensing concepts can effectively compensate for electrical feedthrough due to parasitic impedances at the first mode, providing a deflection signal with sufficiently high dynamic range for tapping-mode AFM imaging. Due to the on-chip electromechanical design, these concepts do not necessitate complicated readout circuits and provide rapid feedthrough cancellation by simply tuning a gain.

The pseudo-differential actuation method demonstrated with the Type I cantilever does not require a separate bottom electrode layer, unlike the differential sensing approach. It can hence be integrated into standard commercial MEMS fabrication processes such as PiezoMUMPs [36], which dictates the use of a physically common ground. One of the drawbacks of this method is that the cancellation of the feedthrough has the effect of also reducing the desired signal level, as shown in Fig. 6c. Additionally, when the pseudo-differential actuation method has been tuned for the first mode, significant levels of feedthrough are still present at the higher modes of the cantilever. This indicates that the out-of-phase feedthrough signal induced via the pseudo actuator is sensitive to higher-order parasitic effects resulting from sources other than the electrode layout, meaning that the feedthrough compensation is less effective over a wider frequency range.

On the other hand, the differential sensing mechanism implemented on the Type II cantilever not only maintains the original signal level better than Type I after cancellation, but it also provides better noise performance (as shown later in Section V-C) and a higher degree of feedthrough cancellation at the higher modes compared to the pseudo-differential actuation method, when tuned for maximum cancellation at the first mode. Unlike the pseudo-differential actuation method, where the parasitic impedances associated with the dummy

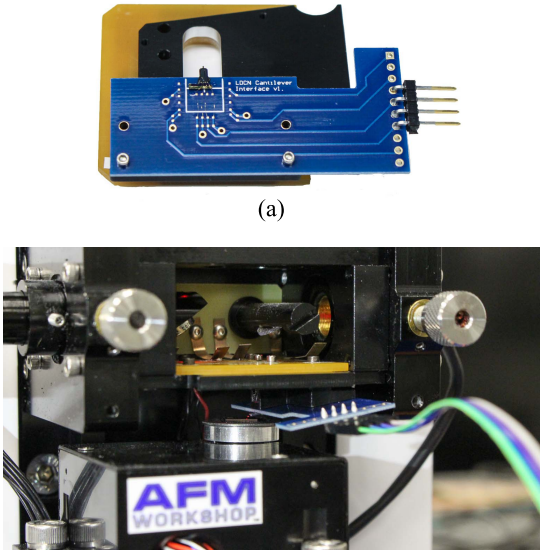

(a) (b)

Fig. 8. The experimental setup used for AFM imaging with the microfabricated cantilevers. (a) A cantilever fixed and wire bonded to an interface PCB, and attached to an AFM probe holder. (b) The cantilever and PCB mounted inside the AFM.

actuator can only approximate those of the actual actuator, the left and right sensors of the differential sensing method are fully symmetric in terms of design as well as material composition. Correspondingly, the tuned differential sensor output is able to more effectively recover the dynamics of the cantilever within a broad bandwidth. This is also supported by a comparison of each cantilevers' phase response. While both sensor outputs undergo a sharp phase transition at resonance, as expected (as shown in Figs. 6a and 6b), the phase response of the Type II cantilever is closer to that of the ideal response, compared with that of the Type I cantilever. This again suggests that it is more effective at compensating for parasitic effects over a wider frequency range. Lastly, as evident from the experimental results (Fig. 7), the gain of 1.38 used in the differential sensing experiments to effectively cancel the feedthrough is very close to the ratio of the left and right sensors' individual dynamic range (1.7 dB/1.2 dB = 1.41). This hints that measuring this ratio provides a highly accurate starting point for the gain tuning to achieve even more systematic and rapid cancellation.

V. AFM Imaging

A. Experimental Setup

Both the Type I and Type II cantilevers are used to obtain tapping-mode AFM images of an NT-MDT TGZ2 calibration grating, which features repeating steps of height 110 ± 2 nm with a period of 3 μm. For these experiments, an AFMWorkshop TT-AFM is used to perform the sample imaging.

The fabricated MEMS cantilevers are fixed to a custom printed circuit board (PCB) providing access to the actuation and sensing electrodes through wire-bonded connections, with the PCB being fixed to a custom-fabricated probe holder. Photos of the experimental setup are shown in Fig. 8.

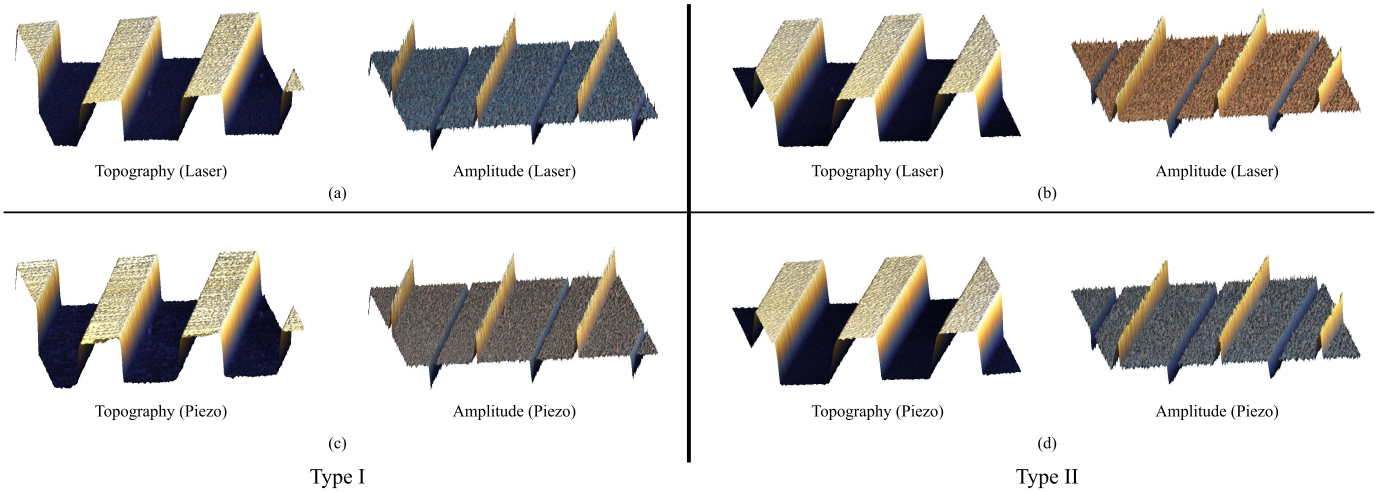

Fig. 9. Tapping-mode AFM images, obtained using the Type I and Type II cantilevers. (a) and (b) are obtained using the AFM's laser detector and photodiode, while (c) and (d) are obtained using the cantilever's integrated piezoelectric sensor.

B. Imaging

In order to investigate the effectiveness and performance of the proposed feedthrough cancellation methods, typical tapping-mode scan parameters have been selected for AFM imaging. Each cantilever is used to obtain $8\,\mu\text{m} \times 8\,\mu\text{m}$ AFM images in tapping mode using a 1 Hz raster scan rate. The cancellation of the electrical feedthrough for each type of cantilever is tuned prior to imaging, as described in Section IV. The actuation signal applied to the integrated piezoelectric actuator on each cantilever is set to obtain a free-air oscillation amplitude of approximately 250 nm at the cantilever's first resonance frequency, with the setpoint amplitude during imaging being set to 45% of this value.

For the purpose of comparison, two AFM images are generated using each cantilever; one image is constructed using the AFM's laser and photodetector to measure the cantilever's deflection for feedback control of the z axis, while the other uses the output of the cantilever's integrated piezoelectric sensor. All other scan parameters, including those of the AFM's z-axis controller, are kept constant between the tests.

The resulting AFM images, providing topography and amplitude information, are shown in Fig. 9 for both the Type I and Type II cantilevers. For both cantilevers, it is evident that the images generated via the output of the piezoelectric sensors are essentially the same as those using the laser signal.

For further comparison, cross sections of the topography images are provided in Fig. 10. As both the laser and piezoelectric sensors have sufficiently high bandwidth to accurately measure the time-varying displacement of the cantilever [17], it can again be seen that there is little difference between the sample profiles obtained using the piezo signal and the laser signal.

C. Signal-to-Noise Ratio

The noise component in the output of each cantilever's piezoelectric sensor is compared with that of the AFM's laser signal by comparing their signal-to-noise ratios (SNRs).

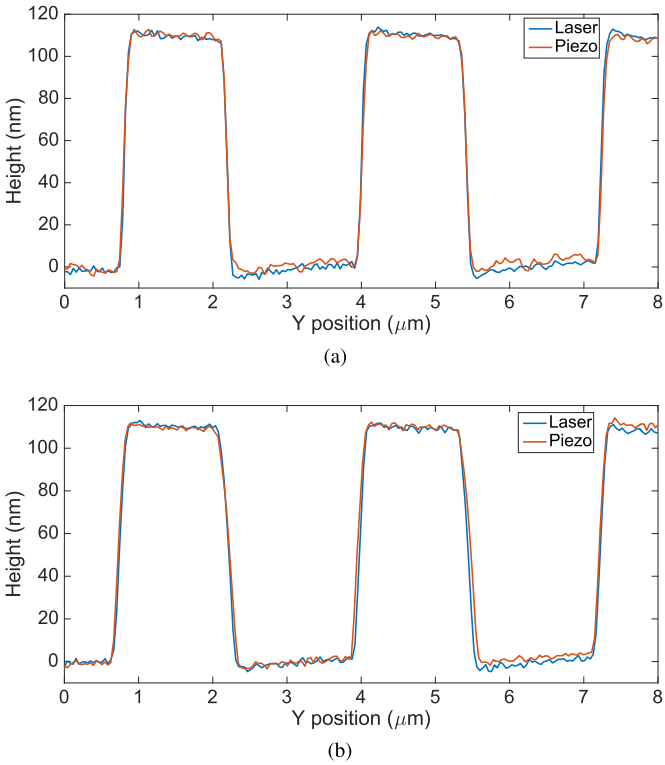

Fig. 10. Cross sections of the AFM topography images obtained via the laser and piezo sensor. (a) Type I cantilever. (b) Type II cantilever.

Each cantilever is excited in free air at its first resonance mode with the same amplitude used for the AFM imaging experiments (approximately 250 nm). The HF2LI lock-in amplifier is then used to demodulate each sensor signal around a bandwidth of 400 Hz and generate an FFT analysis, as shown in Fig. 11. For each figure, the measurements have been normalized by shifting the amplitude of the peak at the oscillation frequency to 0 dB; the SNR is then given by the value of the fitted noise floor.

Based on these measurements, the SNRs for the Type I cantilever are determined to be 106 dB (laser) and 74.1 dB (piezo),

TABLE II
SUMMARY OF THE EXPERIMENTAL RESULTS

Cantilever Design	FTC Method	Parameters	1^{st} Mode	2^{nd} Mode	3^{rd} Mode	4^{th} Mode
Type I	Pseudo-Differential Actuation	**Frequency (kHz)**	49.1	196.0	412.1	624.6
		Dynamic Range (dB)	20.32	2.26	3.80	0.91
		SNR (dB)	74.1	-	-	-
Type II	Differential Sensing	**Frequency (kHz)**	49.7	217.3	428.4	685.3
		Dynamic Range (dB)	34.71	16.62	15.98	30.96
		SNR (dB)	81.7	-	-	-

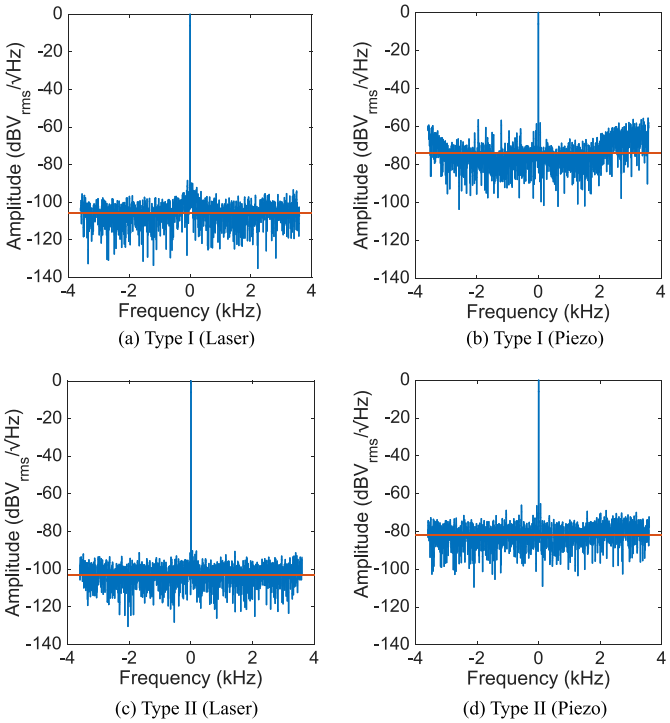

Fig. 11. SNR comparisons using laser and piezo sensing signals. (a) and (b) Type I cantilever. (c) and (d) Type II cantilever.

while for the Type II cantilever they are 103 dB (laser) and 81.7 dB (piezo). It is clear that the signals derived from the piezoelectric sensors provide lower SNRs compared with the use of the laser and photodetector, leading to an effective reduction in vertical imaging resolution (which is nevertheless still sufficient for the grating used in this work). A major contributing factor is the fact that the piezoelectric sensor readout circuits implemented in the current experiment setup are of a prototype nature and are physically separated from the cantilevers with the use of connecting cables. Future work will integrate the sensor readout circuits adjacent to the cantilevers on the same PCB, which will likely reduce the noise present in the output by a significant amount.

Comparing the two cantilevers, the SNR of the Type II cantilever is 7.6 dB higher than that of the Type I cantilever. As noted in Fig. 6, the use of the Type I cantilever's differential actuation scheme has the effect of reducing the amplitude of the sensor signal level, likely accounting for the corresponding reduction in the SNR.

VI. CONCLUSIONS

We have demonstrated the implementation of two on-chip feedthrough cancellation methods to address the common issue of crosstalk in active AFM cantilevers with integrated sensors and actuators. The feedthrough due to the superposition of the actuation signals on the sensor output is drastically reduced by the proposed pseudo-actuation and differential sensing concepts. The concealed dynamics of the cantilevers are recovered through these straightforward methods that allow successful AFM imaging using the on-chip transducers. A summary of the experimental results are demonstrated in Table II.

While both methods are essentially based on tuning and subtracting an inverted version of the feedthrough from the sensing signal by simply using the on-chip elements and differential op-amps, our findings indicate that unlike the pseudo-differential actuation and other cancellation methods in the literature, the differential sensing concept is more effective at recovering the cantilever's dynamics over a wide frequency range, even when tuned only for the fundamental mode. This multi-modal cancellation is especially desirable for multi-frequency AFM applications with active cantilevers.

Importantly, both concepts are applicable to a wide range of systems including resonators, cantilever-based sensors, and other similar microsystems operating at high frequencies with on-chip transducers.

Future work will focus on using the integrated transducers to control the dynamics of the cantilever to obtain faster scan speeds, and integration of the probe tip with the MEMS batch fabrication process.

ACKNOWLEDGMENT

The authors used facilities provided by the University of Texas at Dallas Cleanroom Research Laboratory, to fabricate the cantilevers demonstrated in this work. They acknowledge Dr. Michael G. Ruppert for his assistance with the circuit implementation.

REFERENCES

[1] F. J. Giessibl, "Advances in atomic force microscopy," *Rev. Mod. Phys.*, vol. 75, no. 3, p. 949, Jul. 2003.
[2] N. Jalili and K. Laxminarayana, "A review of atomic force microscopy imaging systems: Application to molecular metrology and biological sciences," *Mechatronics*, vol. 14, no. 8, pp. 907–945, Oct. 2004.
[3] Y. F. Dufrêne, D. Martínez-Martín, I. Medalsy, D. Alsteens, and D. J. Müller, "Multiparametric imaging of biological systems by force-distance curve–based AFM," *Nature Methods*, vol. 10, no. 9, pp. 847–854, 2013.

[4] R. Garcia and E. T. Herruzo, "The emergence of multifrequency force microscopy," *Nature Nanotechnol.*, vol. 7, no. 4, pp. 217–226, Apr. 2012.

[5] T. Ando, "High-speed atomic force microscopy coming of age," *Nanotechnology*, vol. 23, no. 6, p. 062001, 2012.

[6] R. Höper, T. Gesang, W. Possart, O.-D. Hennemann, and S. Boseck, "Imaging elastic sample properties with an atomic force microscope operating in the tapping mode," *Ultramicroscopy*, vol. 60, no. 1, pp. 17–24, 1995.

[7] P. Schön, "Imaging and force probing RNA by atomic force microscopy," *Methods*, vol. 103, pp. 25–33, Jul. 2016.

[8] J. D. Adams, L. Manning, B. Rogers, M. Jones, and S. C. Minne, "Self-sensing tapping mode atomic force microscopy," *Sens. Actuators A, Phys.*, vol. 121, no. 1, pp. 262–266, 2005.

[9] M. Dukic, J. D. Adams, and G. E. Fantner, "Piezoresistive AFM cantilevers surpassing standard optical beam deflection in low noise topography imaging," *Sci. Rep.*, vol. 5, Nov. 2015, Art. no. 16393.

[10] M. Li, H. X. Tang, and M. L. Roukes, "Ultra-sensitive NEMS-based cantilevers for sensing, scanned probe and very high-frequency applications," *Nature Nanotechnol.*, vol. 2, no. 2, pp. 114–120, 2007.

[11] S. C. Minne, S. R. Manalis, A. Atalar, and C. F. Quate, "Contact imaging in the atomic force microscope using a higher order flexural mode combined with a new sensor," *Appl. Phys. Lett.*, vol. 68, no. 10, pp. 1427–1429, 1996.

[12] G. E. Fantner *et al.*, "Use of self-actuating and self-sensing cantilevers for imaging biological samples in fluid," *Nanotechnology*, vol. 20, no. 43, p. 434003, 2009.

[13] C. Lee, T. Itoh, R. Maeda, and T. Suga, "Characterization of micromachined piezoelectric PZT force sensors for dynamic scanning force microscopy," *Rev. Sci. Instrum.*, vol. 68, no. 5, pp. 2091–2100, 1997.

[14] S. C. Minne, S. R. Manalis, and C. F. Quate, "Parallel atomic force microscopy using cantilevers with integrated piezoresistive sensors and integrated piezoelectric actuators," *Appl. Phys. Lett.*, vol. 67, no. 26, pp. 3918–3920, 1995.

[15] S. C. Minne *et al.*, "Automated parallel high-speed atomic force microscopy," *Appl. Phys. Lett.*, vol. 72, no. 18, pp. 2340–2342, 1998.

[16] M. G. Ruppert and S. O. R. Moheimani, "A novel self-sensing technique for tapping-mode atomic force microscopy," *Rev. Sci. Instrum.*, vol. 84, no. 12, p. 125006, 2013.

[17] M. G. Ruppert and S. O. R. Moheimani, "High-bandwidth multimode self-sensing in bimodal atomic force microscopy," *Beilstein J. Nanotechnol.*, vol. 7, no. 1, pp. 284–295, 2016.

[18] M. G. Ruppert and S. O. R. Moheimani, "Multimode Q control in tapping-mode AFM: Enabling imaging on higher flexural eigenmodes," *IEEE Trans. Control Syst. Technol.*, vol. 24, no. 4, pp. 1149–1159, Jul. 2016.

[19] C. Shin, I. Jeon, Z. G. Khim, J. W. Hong, and H. Nam, "Study of sensitivity and noise in the piezoelectric self-sensing and self-actuating cantilever with an integrated wheatstone bridge circuit," *Rev. Sci. Instrum.*, vol. 81, no. 3, p. 035109, 2010.

[20] H.-J. Nam *et al.*, "Calibration of non linear properties of Pb(Zr, Ti)O_3 cantilever using integrated piezoresistive sensor for high speed atomic force microscopy," *Jpn. J. Appl. Phys.*, vol. 41, no. 11B, p. 7153, 2002.

[21] T. Sulchek *et al.*, "Parallel atomic force microscopy with optical interferometric detection," *Appl. Phys. Lett.*, vol. 78, no. 12, pp. 1787–1789, 2001.

[22] S. I. Moore, M. G. Ruppert, and Y. K. Yong, "Multimodal cantilevers with novel piezoelectric layer topology for sensitivity enhancement," *Beilstein J. Nanotechnol.*, vol. 8, pp. 358–371, Feb. 2017.

[23] K. K. Leang, Q. Zou, and S. Devasia, "Feedforward control of piezoactuators in atomic force microscope systems," *IEEE Control Syst.*, vol. 29, no. 1, pp. 70–82, Feb. 2009.

[24] T. Sulchek *et al.*, "High-speed tapping mode imaging with active Q control for atomic force microscopy," *Appl. Phys. Lett.*, vol. 76, no. 11, pp. 1473–1475, 2000.

[25] M. Fairbairn and S. O. R. Moheimani, "Resonant control of an atomic force microscope micro-cantilever for active Q control," *Rev. Sci. Instrum.*, vol. 83, no. 8, p. 083708, 2012.

[26] A. D. L. Humphris, A. N. Round, and M. J. Miles, "Enhanced imaging of DNA via active quality factor control," *Surf. Sci.*, vol. 491, no. 3, pp. 468–472, 2001.

[27] A. G. Fowler, M. Maroufi, and S. O. R. Moheimani, "A silicon-on-insulator microelectromechanical systems probe scanner for on-chip atomic force microscopy," *Rev. Sci. Instrum.*, vol. 86, no. 4, p. 046107, 2015.

[28] M. G. Ruppert, A. G. Fowler, M. Maroufi, and S. O. R. Moheimani, "On-chip dynamic mode atomic force microscopy: A silicon-on-insulator MEMS approach," *J. Microelectromech. Syst.*, vol. 26, no. 1, pp. 215–225, Feb. 2017.

[29] J. E.-Y. Lee and A. A. Seshia, "Parasitic feedthrough cancellation techniques for enhanced electrical characterization of electrostatic microresonators," *Sens. Actuators A, Phys.*, vol. 156, no. 1, pp. 36–42, 2009.

[30] Y. Xu and J. E.-Y. Lee, "Single-device and on-chip feedthrough cancellation for hybrid MEMS resonators," *IEEE Trans. Ind. Electron.*, vol. 59, no. 12, pp. 4930–4937, Dec. 2012.

[31] H. C. Qiu, P. Schwarz, H. Völlm, D. Feili, X. Z. Wu, and H. Seidel, "Electrical crosstalk in two-port piezoelectric resonators and compensation solutions," *J. Micromech. Microeng.*, vol. 23, no. 4, p. 045007, 2013.

[32] M. Maroufi and S. O. R. Moheimani, "A 2DOF SOI-MEMS nanopositioner with tilted flexure bulk piezoresistive displacement sensors," *IEEE Sensors J.*, vol. 16, no. 7, pp. 1908–1917, Apr. 2016.

[33] T. Akiyama *et al.*, "Implementation and characterization of a quartz tuning fork based probe consisted of discrete resonators for dynamic mode atomic force microscopy," *Rev. Sci. Instrum.*, vol. 81, no. 6, p. 063706, 2010.

[34] S. M. Cook, T. E. Schäffer, K. M. Chynoweth, M. Wigton, R. W. Simmonds, and K. M. Lang, "Practical implementation of dynamic methods for measuring atomic force microscope cantilever spring constants," *Nanotechnology*, vol. 17, no. 9, p. 2135, 2006.

[35] J. R. Lozano, D. Kiracofe, J. Melcher, R. García, and A. Raman, "Calibration of higher eigenmode spring constants of atomic force microscope cantilevers," *Nanotechnology*, vol. 21, no. 46, p. 465502, 2010.

[36] A. Cowen, G. Hames, K. Glukh, and B. Hardy, "PiezoMUMPs Design Handbook, Revision 1.3," MEMSCAP Inc., Durham, NC, USA, 2014.

M. Bulut Coskun received the B.Sc. and M.Sc. degrees in mechatronics engineering from Sabanci University, Istanbul, Turkey, in 2009 and 2011, respectively, and the Ph.D. degree in mechanical and aerospace engineering from Monash University, Australia, in 2015. Later on, he joined the Department of Mechanical Engineering, University of Texas at Dallas, as a Research Associate. His current research interests include the design, analysis, fabrication, and characterization of microelectromechanical systems with a particular emphasis on novel microsensors, developing active microcantilevers for high-speed atomic force microscopy applications, and graphene-based sensors.

Anthony G. Fowler (S'10–M'15) received the bachelor's and Ph.D. degrees in electrical engineering from the University of Newcastle, Callaghan, NSW, Australia, in 2010 and 2014, respectively. From 2014 to 2015, he was a Post-Doctoral Fellow at the School of Electrical Engineering and Computer Science, University of Newcastle. He is currently a Research Scientist with the Department of Mechanical Engineering, University of Texas at Dallas, Richardson, TX, USA. His current research interests include the design, fabrication, and analysis of novel microelectromechanical systems for energy harvesting, nanopositioning, and scanning probe microscopy applications.

Mohammad Maroufi (S'14–M'16) received the B.Sc. degrees in mechanical engineering and applied physics as a Distinguished Student and the master's degree in mechatronics from the Amirkabir University of Technology, in 2008 and 2011, respectively, and the Ph.D. degree in electrical engineering from the University of Newcastle, Australia. He is currently a Research Associate with the Department of Mechanical Engineering, University of Texas at Dallas. His research interests include the design and control of MEMS nanopositioning systems, MEMS-based sensing and actuation, on-chip atomic force microscopy, and modeling of smart materials and structures.

S. O. Reza Moheimani (F'11) is currently the James Von Ehr Distinguished Chair in science and technology with the Department of Mechanical Engineering, University of Texas at Dallas. He is also an Adjunct Professor with the University of Newcastle, Australia. His current research interests include ultrahigh-precision mechatronic systems, with particular emphasis on dynamics and control at the nanometer scale, including applications of control and estimation in nanopositioning systems for high-speed scanning probe microscopy and nanomanufacturing, modeling and control of microcantilever-based devices, control of microactuators in microelectromechanical systems, and design, modeling, and control of micromachined nanopositioners for on-chip scanning probe microscopy.

Dr. Moheimani is a fellow of IFAC and the Institute of Physics, U.K. His research has been recognized with a number of awards, including the IFAC Nathaniel B. Nichols Medal in 2014, the IFAC Mechatronic Systems Award in 2013, the IEEE Control Systems Technology Award in 2009, the IEEE TRANSACTIONS ON CONTROL SYSTEMS TECHNOLOGY Outstanding Paper Award in 2007, and several best paper awards from various conferences. He chaired the IFAC Technical Committee on Mechatronic Systems from 2011 to 2017. He is the Editor-in-Chief of *Mechatronics* and has served on the editorial boards of a number of other journals, including the IEEE TRANSACTIONS ON MECHATRONICS, the IEEE TRANSACTIONS ON CONTROL SYSTEMS TECHNOLOGY, and *Control Engineering Practice*.